Severely ill COVID-19 patients display augmented functional properties in SARS-CoV-2-reactive CD8+ T cells

Anthony Kusnadi[1,6], Ciro Ramírez-Suástegui[1,6], Vicente Fajardo[1,6], Serena J Chee[2,6], Benjamin J Meckiff[1], Hayley Simon[1], Emanuela Pelosi[3], Grégory Seumois[1], Ferhat Ay[1], Pandurangan Vijayanand[1,4,5,7], Christian H Ottensmeier[1,4,7].

[1]La Jolla Institute for Immunology, La Jolla, CA, USA.

[2]NIHR and CRUK Southampton Experimental Cancer Medicine Center, Faculty of Medicine, University of Southampton, Southampton, UK.

[3]Southampton Specialist Virology Centre, Department of Infection, University Hospital Southampton NHS Foundation Trust, Southampton, UK.

[4]Liverpool Head and Neck Center, Institute of Translational Medicine, University of Liverpool & Clatterbridge Cancer Center NHS Foundation Trust, Liverpool, United Kingdom

[5]Department of Medicine, University of California San Diego, La Jolla, CA, USA.

[6]These authors jointly contributed to the work

[7]These authors jointly directed the work

Correspondence: P.V. (vijay@lji.org) or C.H.O (cottensmeier@lji.org)

ABSTRACT

The molecular properties of CD8+ T cells that respond to SARS-CoV-2 infection are not fully known. Here, we report on the single-cell transcriptomes of >80,000 virus-reactive CD8+ T cells from 39 COVID-19 patients and 10 healthy subjects. COVID-19 patients segregated into two groups based on whether the dominant CD8+ T cell response to SARS-CoV-2 was 'exhausted' or not. SARS-CoV-2-reactive cells in the exhausted subset were increased in frequency and displayed lesser cytotoxicity and inflammatory features in COVID-19 patients with mild compared to severe illness. In contrast, SARS-CoV-2-reactive cells in the non-exhausted subsets from patients with severe disease showed enrichment of transcripts linked to co-stimulation, pro-survival NF-κB signaling, and anti-apoptotic pathways, suggesting the generation of robust CD8+ T cell memory responses in patients with severe COVID-19 illness. CD8+ T cells reactive to influenza and respiratory syncytial virus from healthy subjects displayed polyfunctional features. Cells with such features were mostly absent in SARS-CoV-2 responsive cells from both COVID-19 patients and healthy controls non-exposed to SARS-CoV-2. Overall, our single-cell analysis revealed substantial diversity in the nature of CD8+ T cells responding to SARS-CoV-2.

INTRODUCTION

Coronavirus infections with SARS-CoV-2 have created a global crisis; a large international effort is underway to develop treatments and vaccines to reduce the severity of disease and to provide protective immunity. To inform this effort, a detailed understanding of anti-viral immune responses is required. CD8+ T cell responses are thought to be critical for control of viral infections[1-4], but to date, our understanding of anti-viral CD8+ T cell responses, specifically against Coronaviridae during infection and in the memory phase, is limited. Recently, studies have begun to improve our knowledge about CD8+ T cells responsive to SARS-CoV-2[5-14], but the molecular features that associate with poor clinical outcomes or differentiate them from other virus-reactive CD8+ T cells remain incompletely understood. We report here on the data generated by single-cell RNA sequencing of virus-reactive CD8+ T cells from COVID-19 patients with varying severity of disease. We benchmark these data against the transcriptomes from CD8+ T cells from healthy donors, who have memory responses to other respiratory viruses.

RESULTS

Evaluation of virus-reactive CD8+ T cells

From 39 subjects with confirmed SARS-CoV-2 infection (17 patients with relatively milder disease not requiring hospitalization, 13 hospitalized patients and 9 additional patients requiring intensive care unit (ICU) support (**Fig. 1a** and **Extended Data Table 1**)), we isolated virus-reactive CD8+ memory T cells using a modified Antigen-Reactive T cell Enrichment (ARTE) assay[15-17]. Peripheral blood mononuclear cells (PBMC) were first stimulated for 24 hours with peptide pools specific to SARS-CoV-2[7,8] (online Methods). Responding cells were then isolated based on the expression of the cell surface activation markers CD137 and CD69 (**Fig. 1a,b** and **Extended Data Fig. 1a**)[5,8,9]. We observed that the numbers of SARS-CoV-2-reactive CD8+ memory T cells were significantly increased in patients with severe COVID-19 illness who required hospitalization compared to those with milder illness not requiring hospitalization (**Fig. 1b**). A large fraction of SARS-CoV-2-reactive CD8+ T cells co-

expressed CD279 (PD-1), CD38, and HLA-DR, which are markers linked to T cell activation and exhaustion[6,18,19] (**Fig. 1c, Extended Data Fig. 1b** and **Extended Data Table 2**). Recent studies in patients with COVID-19 illness have reported that circulating CD8+ T cells express activation markers CD137 and CD69, likely activated by SARS-CoV-2 infection *in vivo*[5,9]; these cells are also captured and contribute to an unbiased evaluation of virus-reactive T cells from patients with recent COVID-19 illness.

To study the properties of SARS-CoV-2-reactive CD8+ T cells in healthy non-exposed individuals[5,20,21], we isolated CD8+ T cells responding to SARS-CoV-2 peptide pools from healthy subjects, who provided blood samples pre-COVID-19 pandemic (**Fig. 1a** and **Extended Data Table 1**). To contextualize our data and to define shared or distinguishing properties of CD8+ T cells reactive with other common non-corona respiratory viruses, we stimulated PBMC from healthy subjects with peptide pools specific to respiratory syncytial virus (RSV) and influenza A (FLU) and isolated responding cells (**Fig. 1a**). In total, from 49 subjects, we sorted and analyzed the single transcriptome and T cell receptor (TCR) sequence of > 87,000 virus-reactive CD8+ T cells with good quality metrics (**Fig. 1a**, **Extended Data Fig. 1c,d** and **Extended Data Table 3**).

Virus-reactive CD8+ T cells show transcriptomic heterogeneity

Our unbiased single-cell transcriptomic analysis of all the virus-reactive CD8+ T cells revealed 8 distinct clusters (**Fig. 2a-c** and **Extended Data Table 4**), indicating that CD8+ memory T cells can activate a wide range of transcriptional programs in response to different viral infections[22]. Recent reports from COVID-19 patients have suggested the presence of exhaustion-related markers in global CD8+ T cell populations. To examine, whether such 'exhausted' cells were present in our dataset, we first generated a consensus list of 'exhaustion' signature genes from 9 studies[23-31] that reported exhaustion features in T cells analyzed from patients with infection or cancer and in mouse models of viral infection (**Extended Data Table 5**). Gene set enrichment analysis (GSEA) of individual clusters showed significant positive enrichment of exhaustion signature genes only in cluster 1 cells (**Fig. 2d-f** and **Extended Data Fig. 2a**). This cluster (cluster 1) was also highly enriched for genes linked to type

I interferon signaling (**Fig. 2d-f** and **Extended Data Fig. 2a**), highlighting the association between the interferon signaling and exhaustion program that has been previously described in the context of murine LCMV infection[32-34]. Because CD4+ T cell-mediated help is required for the generation of robust memory CD8+ T cells[35], we assessed if cells in the 'exhausted' cluster 1 displayed 'unhelped' features that are linked to the lack of CD4+ T cell 'help'[35]. As expected, the exhausted' cluster 1 was also significantly enriched for transcripts linked to 'unhelped' CD8+ T cells (**Fig. 2d,e**). Despite displaying 'exhausted' and 'unhelped' features, intriguingly, cells in cluster 1 showed significant positive enrichment of cytotoxicity signature genes and higher expression levels of cytotoxicity-associated transcripts such as *GZMB* and *GZMA* relative to other clusters (**Fig. 2d-f** and **Extended Data Fig. 2a,b**), which suggested potential heterogeneity within this exhausted subset.

CD8+ T cells reactive to specific viruses made strikingly different contributions to individual clusters (**Fig. 2g** and **Extended Data Table 3**). Clusters 0,1,2, and 3 were overrepresented by SARS-CoV-2-reactive CD8+ T cells from COVID-19 patients, and are likely to reflect memory or effector cells generated in the context of a recent infection. In contrast, the vast majority (>80%) of FLU-reactive and RSV-reactive CD8+ T cells were present in cluster 4, where SARS-CoV-2-reactive cells were underrepresented (<2%) (**Fig. 2g**). Cells in cluster 4 expressed higher levels of transcripts encoding for cytokines such as IFN-γ, TNFα, CCL3, CCL4, XCL1, and XCL2 (**Fig. 2c**, **Extended Data Fig. 2c,** and **Extended Data Table 4**), resembled polyfunctional CD8+ T cells that have been linked to protective immunity against a range of viral infections[36-38 39]. Besides, this cluster displayed positive enrichment and the highest score for genes in the aerobic glycolysis pathway, which is linked to better effector function through multiple mechanisms that are independent of metabolism itself[40,41] (**Fig. 2d,e** and **Extended Data Fig. 2a**).

SARS-CoV-2-reactive CD8+ T cells from healthy non-exposed subjects, presumed to be human coronavirus (CoV)-reactive cells that cross-react with SARS-CoV-2[21], were mainly present in clusters 0,1, 5 and 6 (**Fig. 2g** and **Extended Data Table 3**). The cells in cluster 6 were highly enriched for the expression of transcripts encoding ZNF683 (**Extended Data Fig. 2d**), also known as HOBIT, a

transcription factor that plays a pivotal role in the development of tissue-resident memory (T_{RM}) cells[42]. Notably, the vast majority of cells in cluster 6 were from SARS-CoV-2-reactive cells of healthy non-exposed subjects (**Fig. 2g**); in contrast, cells from COVID-19 patients were mostly absent in this cluster. Overall, our data revealed substantial heterogeneity in the nature of $CD8_+$ T cell subsets generated in response to different viral infections.

Exhausted SARS-CoV-2-reactive $CD8_+$ T cells are increased in mild COVID-19 illness

By linking single-cell transcriptome with T cell receptor (TCR) sequence data of the same cells, we observed extensive clonal expansion as well as clonal sharing of TCRs between the different SARS-CoV-2-reactive subsets in COVID-19 patients (**Fig. 3a,b** and **Extended Data Table 6,7**). Single-cell trajectory analysis showed that cells in cluster 0,1 and 2 were interconnected rather than following a unidirectional path (**Fig. 3c**). Together, our data support both diversity as well as plasticity in the nature of memory $CD8_+$ T cell responses to SARS-CoV-2 infection. However, the dominant memory subsets varied substantially across COVID-19 patients with cells in some subsets represented only by a few patients (**Fig. 3d** and **Extended Data Table 3**). For example, over 85% of SARS-CoV-2-reactive $CD8_+$ T cells in patient 8 were just from cluster 3 (identified by * in **Fig. 3d**), indicating a lack of plasticity in $CD8_+$ T cell responses in this person.

We next examined how SARS-CoV-2-reactive cell subsets varied between patients. COVID-19 patients broadly clustered into two groups based on whether the majority (>50%) of their $CD8_+$ memory T cell responses to SARS-CoV-2 were either from cluster 1 or cluster 0 (**Fig. 3d**). Cluster 1 represented 'exhausted' cells with significant positive enrichment of both exhaustion and interferon signatures, whereas cluster 0 cells showed significant negative enrichment of these signatures, *i.e.*, these cells were not 'exhausted' (**Fig. 2d,e**). Our analysis suggested that a sub-group of COVID-19 patients (30%) mounted a predominantly 'exhausted' $CD8_+$ memory T cell response to SARS-CoV-2. The magnitude of this 'exhausted' response did not show a strong correlation to the time interval between onset of illness and sample collection (**Extended Data Fig. 3a**). Importantly, patients with milder disease had a

significantly higher frequency of cells in the 'exhausted' cluster (cluster 1) when compared to those with severe disease (mean 41% versus 20%, **Fig. 3e**). Further, patients with severe disease when compared to those with mild disease showed significant enrichment of cytotoxicity signature genes and depletion of interferon signature genes in cluster 1 (**Extended Data Fig. 3b,c**), suggesting both quantitative and qualitative differences in cells in the 'exhausted' cluster based on disease severity. In support of qualitative differences, single-cell differential gene expression analysis showed that cells in the 'exhaustion' cluster (cluster 1) from severe COVID-19 patients expressed significantly higher levels of transcripts encoding for cytotoxicity-associated molecules (granzyme B, granzyme H, granulysin, Fas ligand[5,43]) and pro-inflammatory cytokines (CCL3, CCL4, CSF-2, TNF, LTA and LTB)[5,9,44] (**Fig. 3f,g,** and **Extended Data Fig. 3d**)**.** Transcripts encoding for several transcription factors that support cytokine production, inflammation and persistence (T-BET, BHLHE40, NFKB2, REL, FOS, JUNB)[45-50] (**Fig. 3h**,**i** and **Extended Data Table 8**) were also expressed at significantly higher levels in cluster 1 cells from COVID-19 patients with severe illness. TCR sequence analysis of cells in the 'exhausted' cluster 1 revealed greater clonal expansion in patients with severe compared to mild illness, suggesting greater proliferative capacity and/or persistence of cells from severe COVID-19 patients (**Fig. 3i**). Given the importance of exhaustion programs in preventing excessive host tissue damage in viral infections[51,52], we speculate that the failure to imprint an 'exhaustion' program that restrains T cell effector function may reflect a failure to limit exaggerated $CD8_+$ T cell effector function, and thereby contribute to disease pathogenesis in some patients with severe COVID-19 illness.

Pro-survival features in SARS-CoV-2-reactive $CD8_+$ T cells from patients with severe COVID-19

SARS-CoV-2-reactive cells from COVID-19 patients, who did not mount a pre-dominant 'exhausted' response, were present mainly in clusters 0 and 2, the 'non-exhausted' subsets (**Fig. 2d, 3d**). These 'non-exhausted' subsets displayed cytotoxicity signature scores comparable to other clusters (**Fig. 2d**). Furthermore, cluster 2 was enriched for cell cycle signature, indicative of a higher proportion of proliferating cells in this cluster (**Fig. 2c, e**). We found no significant difference in the

proportions of cells in cluster 0 and 2 between patients with severe and mild COVID-19 illness (**Extended Data Fig. 4a**).

However, single-cell differential gene expression analysis in clusters 0, as well as cluster 2, revealed significant transcriptional differences between COVID-19 patients with mild and severe illness (**Fig. 4a** and **Extended Data Table 8**). Ingenuity pathway analysis of transcripts with increased expression in cluster 0 from COVID-19 patients with severe relative to mild illness showed significant enrichment of transcripts in multiple co-stimulation pathways (OX40, CD27, CD28, 4-1BB, CD40), the NF-κB and apoptosis signaling pathways (**Fig. 4b-d**, **Extended Data Fig. 4b-d** and **Extended Data Table 9**). Co-stimulation is required for the robust activation and generation of memory T cell responses[53], and activation of the NFκB pathway is important for T cell IL-2 production, proliferation, survival, cytokine production, and effector function[46]. IL2 receptor alpha and STAT5 encoding transcripts were also increased in severe compared to mild disease, indicating a greater potential for these cells to receive the pro-survival IL-2 signals[54] (**Fig. 4a,c**). Other transcripts with increased expression encoded for transcription factors involved in cell fitness and cytokine production (BHLHE40)[45], effector differentiation (BLIMP1)[55] and prevention of exhaustion (JUN)[49], and for CRTAM that has previously been shown to be important for generating effective cytotoxic T cells and viral clearance in mouse models[56,57] (**Fig. 4a,c,d**). In addition, many transcripts encoding for molecules involved in cell survival and preventing apoptosis like BIRC3, VIM, and BCL2L1[58] were also increased in cells from patients with severe COVID-19 illness, although some molecules with pro-apoptotic function (*e.g.*, BAX, BIM, FAS)[59] were also increased (**Fig. 4a-d** and **Extended Data Fig. 4b**). TCR sequence analysis indicated greater clonal expansion of cells in cluster 0 and 2 from severe COVID-19 patients (**Fig. 4e**). Overall, our findings suggest that SARS-CoV-2-reactive $CD8_+$ T cells from patients with severe COVID-19 displayed multiple features that support the generation of robust $CD8_+$ memory T cell responses with pro-survival properties.

DISCUSSION

Recent studies in COVID-19 patients have verified the presence of CD8+ T cells that are reactive to SARS-CoV-2[5,7,8]. However, the nature and types of CD8+ T cell subsets that respond to SARS-CoV-2 and whether they play an essential role in driving protective or pathogenic immune responses remain elusive. Here, we report on the single-cell transcriptomes and TCR sequence analyses of >87,000 virus-reactive CD8+ T cells from 39 COVID-19 patients and 10 healthy, pre-pandemic donors. To compare the molecular properties of antigen-specific SARS-CoV-2-reactive CD8+ T cells to other common respiratory virus-reactive CD8+ T cells, we also isolated virus-reactive CD8+ T cells from healthy control subjects and analyzed their single-cell transcriptomes.

Across all the virus-reactive CD8+ T cells studied, we delineated eight distinct clusters with distinct transcriptomic features that shared TCRs, suggesting a high degree of plasticity among virus-reactive CD8+ T cells. We find that CD8+ memory T cells can acquire a wide range of transcriptional programs following different viral infections. For example, in healthy subjects, CD8+ T cells with polyfunctional features, linked to protective anti-viral immunity[36-39], are abundant among CD8+ memory T cells reactive to FLU and RSV. In contrast, these cells were mostly absent in SARS-CoV-2 responsive cells from both COVID-19 patients and healthy non-exposed subjects. Notably, cells in this polyfunctional cluster were also significantly enriched for genes related to aerobic glycolysis, which is considered to enhance effector functions of CD8+ memory T cells[40,41].

A large fraction of SARS-CoV-2-reactive cells (43% and 37%) from healthy non-exposed subjects (pre-pandemic), presumed to be human coronaviridae (CoV)-reactive cells that cross-react with SARS-CoV-2 peptide pools[5,21], were present in clusters 1 and 0, respectively. These clusters also had similar representation of SARS-CoV-2-reactive cells from patients with COVID-19 illness. Cells in cluster 1 showed significant positive enrichment for type 1 interferon and ‘exhaustion’ signatures, reminiscent of the ‘exhausted’ CD8+ T cells reported in murine LCMV infection models[60]. Cluster 0, in contrast, was non-exhausted and showed significant negative enrichment of exhaustion and interferon signatures. SARS-CoV-2-reactive cells from COVID-19 patients also contributed the large majority of

cells in cluster 2, which was characterized by enriched expression of cell cycle-related genes. Similar to cells in cluster 0, cluster 2 cells also showed negative enrichment of interferon genes and relatively lower exhaustion signature scores. Thus, we find that the nature of $CD8_+$ T cells reactive to coronaviridae differed substantially from those responding to FLU or RSV.

Intriguingly, COVID-19 patients broadly segregated into two groups, according to whether the majority of the virus-reactive $CD8_+$ memory T cells were in the 'non-exhausted' cluster 0 or the 'exhausted' cluster 1. Patients with mild COVID-19 illness had a greater proportion of SARS-CoV-2-reactive cells in the 'exhausted' cluster 1. Besides, cells in the 'exhausted' subset (cluster 1) from patients with mild COVID-19 illness expressed significantly lesser levels of transcripts encoding for cytotoxicity molecules, Fas ligand and pro-inflammatory cytokines (CCL3, CCL4, CSF-2, TNF, LTA, and LTB)[5,9,43,44], and were significantly less clonally expanded. This finding raises the possibility that the magnitude and quality of the 'exhausted' $CD8_+$ T cell response may be clinically important for limiting excessive tissue damage by SARS-CoV-2-reactive $CD8_+$ T cells in COVID-19 illness.

Qualitative differences also emerged between patients with mild and severe COVID-19 illness in the 'non-exhausted' clusters, cluster 0 and 2. Transcripts increased in cluster 0 cells from patients with severe illness were significantly enriched in multiple co-stimulation pathways (OX40, CD27, CD28, 4-1BB, CD40), NF-κB, and cell survival pathways thought to be important for IL-2 production, proliferation, and survival. This finding suggested that patients with severe disease mount a more effective $CD8_+$ memory T cell response to SARS-CoV-2 infection that could potentially lead to durable protection against re-exposure. Overall, our findings indicate that SARS-CoV-2-reactive $CD8_+$ T cells from patients with severe COVID-19 displayed pro-survival properties and multiple features that potentially support the generation of robust $CD8_+$ memory T cell responses and a lack of restraint reflected in the absence of an 'exhaustion' program. Whether these cells play a role in disease pathogenesis or provide long-term protection is not clear, and further longitudinal analysis and functional studies in relevant model organisms are required to clarify this.

ONLINE METHODS

Patient recruitment, ethics approval, and sample processing

The Ethics Committee of La Jolla Institute (USA) and the Berkshire Research Ethics Committee (UK) 20/SC/0155 provided ethical approval for this study with written consent from all participants. 22 hospitalized patients with reverse transcriptase polymerase chain reaction (RT-PCR) assay confirmed SARS-CoV-2 infection were recruited between April-May 2020. A cohort of 17 non-hospitalized participants was also recruited with RT-PCR assay or serological evidence of SARS-CoV-2 infection. Up to 80 ml of blood was obtained from all subjects for this research. Clinical metadata linked to hospitalized patients such as age, gender, comorbidities, level of clinical care required, radiological findings, and laboratory results are provided in **Extended Data Table 1**. The COVID-19 cohort consisted of 30 (77%) White British/White Other, 4 (10%) Indian, 2 (5%) Black British, 2 Arab (5%), and 1 Chinese (3%) participants. Of the 39 COVID-19 subjects, 22 (56%) had moderate/severe disease requiring hospitalization, and 17 (44%) had mild disease, not requiring hospitalization. The median age of hospitalized patients was 60 (33-82), and 77% were male. The median age of the non-hospitalized participants was 39 (22-50), and 47% were male. To study SARS-CoV-2-, FLU- and RSV-reactive $CD8_+$ T cells from healthy subjects, we utilized de-identified buffy coat samples from 10 healthy adult subjects who donated blood at the San Diego Blood Bank before 2019, prior to the COVID-19 pandemic. Peripheral blood mononuclear cells (PBMC) were isolated from blood by density centrifugation over Lymphoprep (Axis-Shield PoC AS, Oslo, Norway) and cryopreserved in 50% human serum, 40% complete RMPI 1640 medium and 10% DMSO.

Peptide pools

Two overlapping 15-mer SARS-CoV-2 peptide pools were purchased from Miltenyi $Biotec_8$. These peptide pools were derived from the immunodominant sequence of the spike glycoprotein (S) and the complete sequence of the membrane glycoprotein (M) of SARS-CoV-2. For capturing FLU- and RSV-reactive $CD8_+$ T cells, PepTivator Influenza A (H1N1) and RSV strain B1 peptide pools that

covered the entire sequence of Hemagglutinin (HA) and Nucleoprotein (N) of each virus respectively, were obtained from Miltenyi Biotec.

Antigen-reactive T cell enrichment (ARTE) assay

Virus-reactive $CD8_+$ memory T cells were isolated using the protocol from Bacher *et al*. 2016 with minor modifications[15]. Thawed PBMC were plated overnight (5 % CO_2, 37 ˚C) in 1 ml (concentration of 5 x 10_6 cells/ml) of TexMACS medium (Miltenyi Biotec) on 24-well culture plates. Each of the SARS-CoV-2-specific peptide pools (1 µg/ml) were added separately to the PBMC culture for 24 hours. For subsequent magnetic-based enrichment of $CD137_+$ cells, cells were sequentially stained with human serum IgG (Sigma Aldrich) for FcR block, cell viability dye (eFluor780/APC.Cy7, eBioscience), Fluorescence-conjugated antibodies, Cell-hashtag TotalSeq™-C antibody (0.5 µg/condition, clone: LNH-94;2M2, Biolegend), and a biotin-conjugated CD137 antibody (clone REA765; Miltenyi Biotec) followed by anti-biotin microbeads (Miltenyi Biotec). The following fluorescence-conjugated antibodies were used: anti-human CD3 (UCHT1, Biolegend), CD4 (OKT4, Biolegend), CD8B (SIDI8BEE, eBioscience), CD137 (4B4-1, Biolegend), CD69 (FN50, Biolegend), CCR7 (3D12, BD Biosciences), CD45RA (HI100, Biolegend), CD38 (HB-7, Biolegend), HLA-DR (G46-6, BD Biosciences), PD-1 (EH12.1, Biolegend). Antibody-tagged cells were added to MS columns (Miltenyi Biotec) to positively select $CD137_+$ cells. After elution, FACSAria Fusion Cell Sorter (Becton Dickinson) was utilized to sort $CD8_+$ memory T cells expressing CD137 and CD69. **Extended Data Fig. 1a** shows the gating strategy used for sorting. FlowJo software (v10.6.0) was employed for all Flow Cytometry Data analysis. In parallel, virus-reactive $CD4_+$ memory T cells were isolated from the same cultures and analysis of their single-cell transcriptomes reported elsewhere[61].

Cell isolation and single-cell RNA-seq assay (10x platform)

To facilitate the integration of single-cell RNA-seq and TCR-seq profiling from the sorted $CD8_+$ T cells, 10x Genomics 5'TAG v1.0 chemistry was utilized. A maximum of 60,000 virus-reactive $CD8_+$ memory T cells from up to 8 donors was sorted into a low retention 1.5mL collection tube containing

500 µL of a solution of PBS:FBS (1:1) supplemented with RNAse inhibitor (1:100). After sorting, ice-cold PBS was added to make up to a volume of 1400 µl. Cells were then spun down (5 min, 600 g, 4 ˚C), and the supernatant was carefully aspirated, leaving 5 to 10 µl. The cell pellet was gently resuspended in 25 µl of resuspension buffer (0.22 µm filtered ice-cold PBS supplemented with ultra-pure bovine serum albumin; 0.04 %, Sigma-Aldrich). Following that, 33 µl of the cell suspension was transferred to a PCR-tube and single-cell library prepared as per the manufacturer's instructions (10x Genomics).

Single-cell transcriptome analysis

Using 10x Genomics' Cell Ranger software (v3.1.0) and the GRCh37 reference (v3.0.0) genome, reads from single-cell RNA-seq were aligned and collapsed into Unique Molecular Identifiers (UMI) counts. The Feature Barcoding Analysis pipeline from Cell Ranger was used to generate hashtag UMI counts for each TotalSeq™-C antibody-capture library. UMI counts of cell barcodes were first obtained from the raw data output, and barcodes with less than 100 UMI for the most abundant hashtag were filtered out. Donor identities were assigned using Seurat's (v3.1.5)[62] *MULTIseqDemux* (autoThresh = TRUE and maxiter = 10) with the UMI counts. Cell barcodes were classified into three categories: donor ID (singlet), Doublet, Negative enrichment. Singlet cells were then stringently re-classified as doublet if the ratio of UMI counts between the top 2 barcodes was less than 3. All cells that were not classified as doublets or negative were used for downstream analysis. Cells from two COVID-19 patients with mild disease (patient 28 and 48) were not identifiable in the downstream analyses due to the lack of cell hashtags.

Single-cell RNA-Seq libraries (N = 15) were aggregated using Cell Ranger's *aggr* function (v3.1.0). Analysis of the combined data was carried out in the R statistical environment using the package Seurat (v3.1.5). To filter out doublets and to eliminate cells with low-quality transcriptomes, cells were excluded if they were expressing < 800 or > 4400 unique genes, had < 1500 or > 20,000 total UMI content, and > 10% of mitochondrial UMIs. The summary statistics for each single-cell

transcriptome library are given in **Extended Data Table 3** and show good quality data with no major differences in quality control metrics between batches (**Extended Data Fig. 1c**). Only transcripts expressed in at least 0.1% of the cells were included for further analysis. Using default settings in Seurat software, the filtered transcriptome data was then normalized (by a factor of 10,000) and log-transformed per cell. The top variable genes with a mean expression greater than 0.01 counts per million (CPM) and explaining 25% of the total variance were selected using the Variance Stabilizing Transformation method[62]. The transcriptomic data was then further scaled by regressing the number of UMIs detected, and the percentage of mitochondrial counts per cell. Principal component analysis was performed using the top variable genes, and based on the standard deviation of the principal components portrayed as an "elbow plot", the first 25 principal components (PCs) were selected for downstream analyses. Cells were clustered using the *FindNeighbors,* and *FindClusters* functions in Seurat with a resolution of 0.2. The robustness of clustering was verified by other clustering methods and by modifying the number of PCs and variable genes utilized for clustering. Analysis of clustering patterns of SARS-CoV-2-reactive $CD8^+$ T cells across multiple batches revealed no evidence of strong batch effects (**Extended Data Fig. 1d**). Plots to visualize normalized UMI data were created using the Seurat package and custom R scripts.

Single-cell differential gene expression analysis

MAST package in R (v1.8.2)[63] was used to perform pair-wise single-cell differential gene expression analysis after converting UMI data to $\log_2(\text{CPM}+1)$. For genes to be considered differentially expressed, the following thresholds were used: Benjamini-Hochberg–adjusted *P*-value < 0.05 and a $\log_2$ fold change greater than 0.25. Cluster markers (transcripts enriched in a given cluster) were determined using the function *FindAllMarkers* from Seurat.

Gene Set Enrichment Analysis and Signature Module Scores

Signature lists were extracted from published data sets and databases. Gene names from murine datasets were converted to human gene names using the biomaRt R package. Gene lists were

then filtered to exclude genes that were expressed (CPM > 0) in < 2 % of the cells. Exhaustion consensus signature list was derived by considering genes that were present in > 3 exhaustion signature datasets[23-31] (**Extended Data Table 5**). Genes that were present in cytotoxicity signatures[23,64] or viral activation signatures[57] were then excluded from this consensus list. The R package *fgsea* was used to calculate the GSEA scores with the signal-to-noise ratio as a metric. Default parameters other than minSize = 3 and maxSize = 500 were used. Normalized enrichment scores were presented as enrichment plots.

Signature scores were estimated with the Seurat's *AddModuleScore* function, using default settings. For a given cell, each signature score is defined by the mean of the gene list of interest minus the mean expression of control gene lists. Control gene lists were sampled (size equal to the signature list) from bins defined based on the level of expression of the genes in the signature list. Signature gene lists used for analysis are provided in **Extended Data Table 5**.

Single-cell trajectory analysis

Monocle 3 (v0.2.1)[65] was used to calculate the "branched" trajectory; settings included the number of UMI and percentage of mitochondrial UMI as the model formula, and taking the highly variable genes from Seurat for consistency. After using the PCA output from Seurat and allocating a single partition for all cells, the cell-trajectory was outlined on the UMAP generated from Seurat as well. The 'root' was assigned using the *get_earliest_principal_node* function given in the package's tutorial.

T cell receptor (TCR) sequence analysis

Single-cell libraries enriched for V(D)J TCR sequences were processed to get clonotype information for each independent sample with the *vdj* pipeline from Cell Ranger (v3.1.0 and human annotations reference GRCh38, v3.1.0, as recommended). Joint analysis of single-cell transcriptomes and TCR repertoires was performed by aggregating independent libraries through custom scripts. For this purpose, cell barcodes were matched between corresponding libraries from each type. Then, each

unique clonotype, a set of productive Complementarity-Determining Region 3 (CDR3) sequences as defined by 10x Genomics, was identified across all library annotations files. Finally, clone statistics, mainly clonotypes' frequencies, and proportions were recalculated for the whole aggregation (considering only cells found in both modalities) so that previously-identified good quality cells were annotated with a specific clonotype ID and such clone statistics. Clone size was calculated as the number of cells expressing a given clonotype ID, and a clonotype was called as clonally expanded if this value was greater than 1 (clone size ≥ 2). Clone size was depicted on UMAP (per cell) or violin plots (per group, where color indicated clone size median of each group) using custom scripts, and clonotype sharing was presented using the tools from UpSetR[66].

Ingenuity Pathway Analysis (IPA)

IPA was performed using the default setting (v01-16) on transcripts that were significantly increased in expression in cluster 0 cells from patients with severe COVID-19 illness compared to mild illness. The canonical pathway analysis was performed to elucidate the enriched pathways in this data set and to visualize and highlight the gene overlap between the given data set with a particular enriched pathway. The upstream regulator network analysis was used to identify and visualize the interactions between differentially expressed downstream target genes in a given dataset with a particular upstream regulator.

Statistical Analysis

Graphpad Prism 8.4.3 software was utilized for relevant data statistical analysis. Detailed information regarding statistical analysis, including test types and number of batches or samples is provided in the figure legends. P values are specified in the text or the figure legends. The data normality tests were performed, and for data that fell within Gaussian distribution, appropriate parametric statistical tests were performed. For those that did not conform to the equal variance-Gaussian distribution, appropriate non-parametric statistical tests were used.

Data Availability

Scripts to obtain figures and tables provided in the manuscript are available in our repository on GitHub (https://github.com/vijaybioinfo/COVID19_2020). Sequencing data for this study has been deposited into the Gene Expression Omnibus under GSE153931.

ACKNOWLEDGMENTS

We thank Luke Smith for patient recruitment and sample collection; Callum Dixon, Benjamin Johnson, Lydia Scarlett, and Silvia Austin for collection of clinical data; Céline Galloway, Oliver Wood, Katy McCann and Lindsey Chudley for sample processing. We thank the La Jolla Institute (LJI) Flow Cytometry Core for assisting with cell sorting; the LJI's Clinical Studies Core for organizing sample collection. We thank Alessandro Sette for provided essential reagents for optimizing isolation of viral-reactive $CD8_+$ T cells. Peter Friedmann and Anusha Preethi Ganesan for providing critical feedback on the manuscript. This work was funded by NIH grants U19AI142742, U19AI142742-02S1 (P.V., C.H.O), U19AI118626 (P.V., G.S.), R01HL114093 (P.V., F.A., G.S.,), R35-GM128938 (F.A), S10RR027366 (BD FACSAria-II), S10OD025052 (Illumina Novaseq6000), the William K. Bowes Jr Foundation (P.V.), and Whittaker foundation (P.V., C.H.O.). Supported by the Wessex Clinical Research Network and National Institute of Health Research UK.

AUTHOR CONTRIBUTIONS

A.K., S.J.C., C.H.O., and P.V. conceived the work. A.K., S.J.C, C.H.O., and P.V. designed the study and wrote the manuscript. S.J.C supervised patient identification, recruitment, sample collection and processing. E.P., supervised the analysis of viral PCR and serology tests. A.K. and B.M., performed ARTE assay and FACS sorting, and H.S., performed single-cell RNA-sequencing under the supervision of C.H.O., and P.V. C.R.S. and V.F.R, performed bioinformatic analyses under the supervision of G.S., F.A., C.H.O., and P.V.

COMPETING FINANCIAL INTERESTS

The authors declare no competing financial interests.

FIGURE LEGENDS

Figure 1. CD8+ T cell responses in COVID-19 illness

a, Study design overview. **b**, Representative FACS plots displaying surface staining of CD137 and CD69 in post-enriched CD8+ memory T cells, stimulated for 24 hours with SARS-CoV-2 peptide pools, from COVID-19 patients with mild and severe illness (left), and summary of the number of cells sorted per million PBMC (right). **c**, Representative FACS plots (left) showing surface expression of PD-1 in CD8+ memory T cells *ex vivo* (without *in vitro* stimulation) and in CD137+CD69+ CD8+ memory T cells following stimulation, post-enrichment (CD137-based) and corresponding summary plots (right) showing proportion of PD-1 expressing cells in each study subject (P = 0.26, unpaired t-test); Data are displayed as mean +/- S.E.M (N=39). ***P<0.001 by Mann-Whitney test (**b**).

Figure 2. Virus-reactive CD8+ T cells show transcriptomic heterogeneity

a, Uniform manifold approximation and projection (UMAP) analysis that displays single-cell transcriptomic landscape of sorted CD137+CD69+ CD8+ memory T cells following 24 hours stimulation with virus-specific peptide pools. Seurat-based clustering of single cells colored based on cluster type. **b**, Heatmap showing expression of the most significantly enriched transcripts in clusters 0-6 (see **Extended Data Table 4**, Seurat marker gene analysis – comparison of a cluster of interest versus all other cells). Shown are a subset of the top 200 transcripts that have an adjusted P < 0.05, $\log_2$ fold change > 0.25, and >10% difference in the percentage of cells expressing the differentially expressed transcript between two groups compared. **c**, Graph showing average expression and percent expression of selected marker transcripts in each cluster; cells in cluster 7 that comprise <1% of all cells are not shown (**b,c**). **d**, UMAP is illustrating exhaustion, interferon (IFN) response, cytotoxicity, 'unhelped', and glycolysis signature scores for each cell. **e**, Gene Set Enrichment Analysis (GSEA) for the indicated signature genes comparing each cluster with the rest of the cells. Heatmap shows summary of the normalized enrichment scores for each cluster. Gray color indicates that the signature

does not reach statistical significance (*P* >0.05) in a given cluster. **f**, Violin plots showing expression of representative exhaustion, IFN response, cytotoxicity marker transcripts (*LAG3*, *MX1*, *GZMB*, respectively) in cluster 1 compared to an aggregation of remaining cells (Rest). The color indicates percentage of cells expressing indicated transcript. **g**, UMAPs are depicting $CD8_+$ memory T cells for individual virus-specific pool stimulation conditions (top panel). Each group of virus-reactive cells was randomly downsampled to ensure equal representation, corresponding pie charts, displaying proportions of virus-reactive cells in individual clusters (bottom panel).

Figure 3. Exhausted SARS-CoV-2-reactive $CD8_+$ T cells are increased in mild COVID-19 illness

a, Single-cell TCR sequence analysis of SARS-CoV-2-reactive cells showing the sharing of TCRs between cells from individual clusters (rows, connected by lines). Bars (top) indicate the number of cells intersecting indicated clusters (columns). **b**, UMAP is showing the clone size of SARS-CoV-2-reactive cells from COVID-19 patients. **c**, Single-cell trajectory analysis showing the relationship between cells in different clusters (line). **d**, Unsupervised clustering of all COVID-19 patients (mild and severe illness) based on the proportion of SARS-CoV-2-reactive $CD8_+$ T cells present in each cluster per patient. The symbol * below represents patient 8. Clusters 4, 6, and 7 that had a very low frequency of cells in COVID-19 patients (<1% cells per cluster in total) are not shown here, full details provided in **Extended Data Table 3**. **e**, Bar chart comparing the proportion of cells in cluster 1 from COVID-19 patients with mild and severe illness. Data are displayed as mean +/- S.E.M (N=37, 2 subjects without hashtag data were not included for donor-specific analysis). **f**, Volcano plot showing genes differentially expressed (adjusted *P* < 0.05, mean CPM >0, $\log_2$ fold change >0.25) in cluster 1 cells between COVID-19 patients with severe and mild disease. **g**, Violin, and dot plots comparing the expression of indicated transcripts in cluster 1 cells between COVID-19 patients with mild and severe disease. **h**, Plot displaying the expression of several key transcription factors in cluster 1 cells from COVID-19 patients with severe and mild illness. **i**, Violin plots showing the degree of $CD8_+$ T cell-clonal expansion in cluster 1 cells between COVID-19 patients with mild and severe disease. **P*<0.05, *****P*<0.0001 by Mann-Whitney tests (**e**,**i**).

Figure 4. Pro-survival features in SARS-CoV-2-reactive CD8+ T cells from patients with severe COVID-19 illness

a, Plot shows fold change values of differentially expressed genes (adjusted $P < 0.05$, mean CPM >0, $\log_2$ fold change >0.25) in cluster 0 (x-axis) and 2 (y-axis) when comparing COVID-19 patients with severe and mild illness. A positive value indicates that the particular gene has increased expression in patients with severe disease relative to patients with mild disease in a given cluster, while a negative value indicates the opposite. **b-d**, Ingenuity pathway analysis (IPA) of genes with increased expression (adjusted P <0.05, $\log_2$ fold change >0.25) in cluster 0 cells between COVID-19 patients with severe versus mild illness; **b**, Top 16 canonical pathways with significant enrichment; **c**, Upstream regulatory network analysis of genes in NF-κB pathway; **d**, Transcripts encoding components in the 4-1BB and OX40 signaling pathway. **e**, Violin plots showing the degree of CD8+ T cell-clonal expansion in cluster 0 and 2 between COVID-19 patients with mild and severe disease. **** P <0.0001 by Mann-Whitney test.

Extended Data Figure Legends

Extended Data Figure 1. CD8+ T cell responses in COVID-19 illness

a, Gating strategy to sort: lymphocytes size-scatter gate, single cells (Height vs Area forward scatter (FSC)), live, CD3+CD8+ memory (CD45RA+CCR7+ naïve cells excluded) activated CD137+ CD69+ cells. Surface expression of activation markers was analyzed on CD8+ memory T cells. **b**, Representative FACS plots (left) showing surface expression of CD38 and HLA-DR in CD8+ memory T cells *ex vivo* and in CD137+CD69+ CD8+ memory T cells following 24 hours of stimulation, post-enrichment (CD137-based), and summary of proportions of cells expressing CD38 (N=39, P=0.24 by Mann-Whitney test)) and HLA-DR (N=34, P=0.11 by Mann-Whitney test) in CD137+CD69+ CD8+ memory T cells following stimulation and post-enrichment (CD137-based) in COVID-19 patients with mild and severe disease

(right); Data are mean +/- S.E.M. **c**, Number of genes recovered for each 10X library sequenced. **d**, Distribution of cells in each cluster for the 6 batches of SARS-CoV2-reactive CD8+ T cells from COVID-19 patients (right panel).

Extended Data Figure 2. **Virus-reactive CD8+ T cells show transcriptomic heterogeneity**

a, Violin plots showing enrichment patterns of exhaustion, interferon (IFN) response, cytotoxicity, 'unhelped', and glycolysis gene signatures for each cluster. Color indicates signature scores. **b**, Violin plots showing expression of exhaustion and cytotoxicity gene markers in cluster 1 compared to an aggregation of remaining cells (Rest). **c**, Scatter plots (top panel) displaying co-expression of *IFNG* and *TNF, IFNG* and *CCL4*, *XCL1* and *XCL2* transcripts in virus-reactive CD8+ memory T cells in cluster 4 compared to the rest of the cells (Rest). Numbers indicate the percentage of cells in each quadrant. Violin plots (bottom panel) showing expression of indicated transcripts in cluster 4 compared to an aggregation of remaining cells (Rest). **d**, Violin plot showing expression of *ZNF683* in cluster 6 compared to an aggregation of remaining cells (Rest). Color indicates percentage of cells expressing indicated transcript.

Extended Data Figure 3. **Exhausted SARS-CoV-2-reactive CD8+ cells are increased in mild COVID-19 illness**

a, Plot depicting correlation of the proportion of cells in cluster 1 per COVID-19 patients (y-axis, percent) and the interval between symptom onset to blood collection (x-axis, days). R=0.3 (Pearson correlation), P<0.07 (ns). **b,** Gene Set Enrichment Analysis (GSEA) of Interferon response, Cytotoxicity, and Exhaustion signatures in cluster 1 cells between COVID-19 patients with severe versus mild illness. **c**, Violin plots depicting several IFN response genes in cluster 1 cells from COVID-19 patients with mild and severe illness. **d**, Scatter plot displaying co-expression of *TNF* and *CSF2* transcripts in cluster 1 cells from COVID-19 patients with mild and severe illness. Numbers indicate the percentage of cells in each quadrant. **e**, Violin plots comparing the expression of indicated transcripts between *BHLHE40*-expressing and non-expressing cells in cluster 1 from COVID-19 patients with severe disease.

Extended Data Figure 4. Pro-survival features in SARS-CoV-2-reactive CD8+ T cells from patients with severe COVID-19

a, Bar charts comparing the proportion of cells in cluster 0 (P = 0.29 by Mann-Whitney test) and 2 (P = 0.13 by Mann-Whitney test) from COVID-19 patients with mild and severe disease. Data are displayed as mean +/- S.E.M (N=37). **b,** Ingenuity pathway analysis (IPA) of genes with increased expression (adjusted P <0.05, $\log_2$ fold change >0.25) in cluster 0 cells between COVID-19 patients with severe versus mild illness; transcripts encoding components of apoptosis signaling pathway are shown.

EXTENDED DATA TABLES

Extended Data Table 1. Human subject details

Extended Data Table 2. Summary of all FACS data

Extended Data Table 3. Single-cell sequencing quality controls and subject-specific cell numbers

Extended Data Table 4. Single-cell cluster enriched transcripts

Extended Data Table 5. Gene lists utilized for Gene Set Enrichment Analysis and Signature Module Scores

Extended Data Table 6. Subject-specific TCR clonotype data

Extended Data Table 7. Cluster-specific TCR clonotype data

Extended Data Table 8. Single-cell differential gene expression analysis

Extended Data Table 9. Ingenuity Pathway Analysis

REFERENCES

1. Hanke, T., *et al.* Enhancement of MHC class I-restricted peptide-specific T cell induction by a DNA prime/MVA boost vaccination regime. *Vaccine* **16**, 439-445 (1998).
2. McMichael, A., Mwau, M. & Hanke, T. HIV T cell vaccines, the importance of clades. *Vaccine* **20**, 1918-1921 (2002).
3. Arunachalam, P.S., *et al.* T cell-inducing vaccine durably prevents mucosal SHIV infection even with lower neutralizing antibody titers. *Nat Med* (2020).
4. Petitdemange, C., *et al.* Vaccine induction of antibodies and tissue-resident CD8+ T cells enhances protection against mucosal SHIV-infection in young macaques. *JCI Insight* **4**(2019).
5. Grifoni, A., *et al.* Targets of T Cell Responses to SARS-CoV-2 Coronavirus in Humans with COVID-19 Disease and Unexposed Individuals. *Cell* (2020).
6. Thevarajan, I., *et al.* Breadth of concomitant immune responses prior to patient recovery: a case report of non-severe COVID-19. *Nat Med* **26**, 453-455 (2020).
7. Braun, J., *et al.* Presence of SARS-CoV-2 reactive T cells in COVID-19 patients and healthy donors. *medRxiv*, 2020.2004.2017.20061440 (2020).
8. Thieme, C.J., *et al.* The SARS-CoV-2 T-cell immunity is directed against the spike, membrane, and nucleocapsid protein and associated with COVID 19 severity. *medRxiv*, 2020.2005.2013.20100636 (2020).
9. Weiskopf, D., *et al.* Phenotype and kinetics of SARS-CoV-2-specific T cells in COVID-19 patients with acute respiratory distress syndrome. *Sci Immunol* **5**(2020).
10. Laing, A.G., *et al.* A consensus Covid-19 immune signature combines immuno-protection with discrete sepsis-like traits associated with poor prognosis. *medRxiv*, 2020.2006.2008.20125112 (2020).
11. Peng, Y., *et al.* Broad and strong memory CD4 (+) and CD8 (+) T cells induced by SARS-CoV-2 in UK convalescent COVID-19 patients. *bioRxiv* (2020).
12. Daamen, A.R., *et al.* Comprehensive Transcriptomic Analysis of COVID-19 Blood, Lung, and Airway. *bioRxiv*, 2020.2005.2028.121889 (2020).
13. Sekine, T., *et al.* Robust T cell immunity in convalescent individuals with asymptomatic or mild COVID-19. *bioRxiv*, 2020.2006.2029.174888 (2020).
14. Chua, R.L., *et al.* COVID-19 severity correlates with airway epithelium-immune cell interactions identified by single-cell analysis. *Nat Biotechnol* (2020).
15. Bacher, P., *et al.* Regulatory T Cell Specificity Directs Tolerance versus Allergy against Aeroantigens in Humans. *Cell* **167**, 1067-1078 e1016 (2016).
16. Bacher, P., *et al.* Human Anti-fungal Th17 Immunity and Pathology Rely on Cross-Reactivity against Candida albicans. *Cell* **176**, 1340-1355 e1315 (2019).
17. Bacher, P., *et al.* Antigen-reactive T cell enrichment for direct, high-resolution analysis of the human naive and memory Th cell repertoire. *J Immunol* **190**, 3967-3976 (2013).
18. Diao, B., *et al.* Reduction and Functional Exhaustion of T Cells in Patients With Coronavirus Disease 2019 (COVID-19). *Front Immunol* **11**, 827 (2020).
19. Mathew, D., *et al.* Deep immune profiling of COVID-19 patients reveals patient heterogeneity and distinct immunotypes with implications for therapeutic interventions. *bioRxiv* (2020).
20. Thiel, V. & Weber, F. Interferon and cytokine responses to SARS-coronavirus infection. *Cytokine Growth Factor Rev* **19**, 121-132 (2008).
21. Stervbo, U., Rahmann, S., Roch, T., Westhof, T.H. & Babel, N. SARS-CoV-2 reactive T cells in uninfected individuals are likely expanded by beta-coronaviruses. *bioRxiv*, 2020.2007.2001.182741 (2020).
22. Chng, M.H.Y., *et al.* Large-Scale HLA Tetramer Tracking of T Cells during Dengue Infection Reveals Broad Acute Activation and Differentiation into Two Memory Cell Fates. *Immunity* **51**, 1119-1135 e1115 (2019).
23. Guo, X., *et al.* Global characterization of T cells in non-small-cell lung cancer by single-cell sequencing. *Nat Med* **24**, 978-985 (2018).

24. Tirosh, I., *et al.* Dissecting the multicellular ecosystem of metastatic melanoma by single-cell RNA-seq. *Science* **352**, 189-196 (2016).
25. Li, H., *et al.* Dysfunctional CD8 T Cells Form a Proliferative, Dynamically Regulated Compartment within Human Melanoma. *Cell* **176**, 775-789 e718 (2019).
26. Zheng, C., *et al.* Landscape of Infiltrating T Cells in Liver Cancer Revealed by Single-Cell Sequencing. *Cell* **169**, 1342-1356 e1316 (2017).
27. Sade-Feldman, M., *et al.* Defining T Cell States Associated with Response to Checkpoint Immunotherapy in Melanoma. *Cell* **175**, 998-1013 e1020 (2018).
28. Wolski, D., *et al.* Early Transcriptional Divergence Marks Virus-Specific Primary Human CD8(+) T Cells in Chronic versus Acute Infection. *Immunity* **47**, 648-663 e648 (2017).
29. Khan, O., *et al.* TOX transcriptionally and epigenetically programs CD8(+) T cell exhaustion. *Nature* **571**, 211-218 (2019).
30. Singer, M., *et al.* A Distinct Gene Module for Dysfunction Uncoupled from Activation in Tumor-Infiltrating T Cells. *Cell* **166**, 1500-1511 e1509 (2016).
31. Yao, C., *et al.* Single-cell RNA-seq reveals TOX as a key regulator of CD8(+) T cell persistence in chronic infection. *Nat Immunol* **20**, 890-901 (2019).
32. Wu, T., *et al.* The TCF1-Bcl6 axis counteracts type I interferon to repress exhaustion and maintain T cell stemness. *Sci Immunol* **1**(2016).
33. Teijaro, J.R., *et al.* Persistent LCMV infection is controlled by blockade of type I interferon signaling. *Science* **340**, 207-211 (2013).
34. Wilson, E.B., *et al.* Blockade of chronic type I interferon signaling to control persistent LCMV infection. *Science* **340**, 202-207 (2013).
35. Cullen, J.G., *et al.* CD4(+) T help promotes influenza virus-specific CD8(+) T cell memory by limiting metabolic dysfunction. *Proc Natl Acad Sci U S A* **116**, 4481-4488 (2019).
36. Harari, A., *et al.* Skewed association of polyfunctional antigen-specific CD8 T cell populations with HLA-B genotype. *Proc Natl Acad Sci U S A* **104**, 16233-16238 (2007).
37. Tan, A.C., *et al.* Polyfunctional CD8(+) T cells are associated with the vaccination-induced control of a novel recombinant influenza virus expressing an HCV epitope. *Antiviral Res* **94**, 168-178 (2012).
38. Akondy, R.S., *et al.* The yellow fever virus vaccine induces a broad and polyfunctional human memory CD8+ T cell response. *J Immunol* **183**, 7919-7930 (2009).
39. Lachmann, R., *et al.* Polyfunctional T cells accumulate in large human cytomegalovirus-specific T cell responses. *J Virol* **86**, 1001-1009 (2012).
40. Salmond, R.J. mTOR Regulation of Glycolytic Metabolism in T Cells. *Front Cell Dev Biol* **6**, 122 (2018).
41. Jung, J., Zeng, H. & Horng, T. Metabolism as a guiding force for immunity. *Nat Cell Biol* **21**, 85-93 (2019).
42. Mackay, L.K., *et al.* Hobit and Blimp1 instruct a universal transcriptional program of tissue residency in lymphocytes. *Science* **352**, 459-463 (2016).
43. Liao, M., *et al.* Single-cell landscape of bronchoalveolar immune cells in patients with COVID-19. *Nat Med* **26**, 842-844 (2020).
44. Cao, X. COVID-19: immunopathology and its implications for therapy. *Nat Rev Immunol* **20**, 269-270 (2020).
45. Emming, S., *et al.* A molecular network regulating the proinflammatory phenotype of human memory T lymphocytes. *Nat Immunol* **21**, 388-399 (2020).
46. Gerondakis, S. & Siebenlist, U. Roles of the NF-kappaB pathway in lymphocyte development and function. *Cold Spring Harb Perspect Biol* **2**, a000182 (2010).
47. Li, C., *et al.* The Transcription Factor Bhlhe40 Programs Mitochondrial Regulation of Resident CD8(+) T Cell Fitness and Functionality. *Immunity* **51**, 491-507 e497 (2019).
48. Lin, C.C., *et al.* Bhlhe40 controls cytokine production by T cells and is essential for pathogenicity in autoimmune neuroinflammation. *Nat Commun* **5**, 3551 (2014).
49. Lynn, R.C., *et al.* c-Jun overexpression in CAR T cells induces exhaustion resistance. *Nature* **576**, 293-300 (2019).

50. Sullivan, B.M., Juedes, A., Szabo, S.J., von Herrath, M. & Glimcher, L.H. Antigen-driven effector CD8 T cell function regulated by T-bet. *Proc Natl Acad Sci U S A* **100**, 15818-15823 (2003).
51. Ou, R., Zhang, M., Huang, L. & Moskophidis, D. Control of virus-specific CD8+ T-cell exhaustion and immune-mediated pathology by E3 ubiquitin ligase Cbl-b during chronic viral infection. *J Virol* **82**, 3353-3368 (2008).
52. Rouse, B.T. & Sehrawat, S. Immunity and immunopathology to viruses: what decides the outcome? *Nat Rev Immunol* **10**, 514-526 (2010).
53. Duttagupta, P.A., Boesteanu, A.C. & Katsikis, P.D. Costimulation signals for memory CD8+ T cells during viral infections. *Crit Rev Immunol* **29**, 469-486 (2009).
54. Kalia, V. & Sarkar, S. Regulation of Effector and Memory CD8 T Cell Differentiation by IL-2-A Balancing Act. *Front Immunol* **9**, 2987 (2018).
55. Nutt, S.L., Fairfax, K.A. & Kallies, A. BLIMP1 guides the fate of effector B and T cells. *Nat Rev Immunol* **7**, 923-927 (2007).
56. Takeuchi, A.*, et al.* CRTAM confers late-stage activation of CD8+ T cells to regulate retention within lymph node. *J Immunol* **183**, 4220-4228 (2009).
57. Fuchs, Y.F.*, et al.* Gene Expression-Based Identification of Antigen-Responsive CD8(+) T Cells on a Single-Cell Level. *Front Immunol* **10**, 2568 (2019).
58. Zhan, Y., Carrington, E.M., Zhang, Y., Heinzel, S. & Lew, A.M. Life and Death of Activated T Cells: How Are They Different from Naive T Cells? *Front Immunol* **8**, 1809 (2017).
59. Weant, A.E.*, et al.* Apoptosis regulators Bim and Fas function concurrently to control autoimmunity and CD8+ T cell contraction. *Immunity* **28**, 218-230 (2008).
60. Zehn, D. & Wherry, E.J. Immune Memory and Exhaustion: Clinically Relevant Lessons from the LCMV Model. *Adv Exp Med Biol* **850**, 137-152 (2015).
61. Meckiff, B.J.*, et al.* Single-cell transcriptomic analysis of SARS-CoV-2 reactive CD4+ T cells. *bioRxiv* (2020).
62. Stuart, T.*, et al.* Comprehensive Integration of Single-Cell Data. *Cell* **177**, 1888-1902 e1821 (2019).
63. Finak, G.*, et al.* MAST: a flexible statistical framework for assessing transcriptional changes and characterizing heterogeneity in single-cell RNA sequencing data. *Genome Biol* **16**, 278 (2015).
64. Jerby-Arnon, L.*, et al.* A Cancer Cell Program Promotes T Cell Exclusion and Resistance to Checkpoint Blockade. *Cell* **175**, 984-997 e924 (2018).
65. Trapnell, C.*, et al.* The dynamics and regulators of cell fate decisions are revealed by pseudotemporal ordering of single cells. *Nat Biotechnol* **32**, 381-386 (2014).
66. Conway, J.R., Lex, A. & Gehlenborg, N. UpSetR: an R package for the visualization of intersecting sets and their properties. *Bioinformatics* **33**, 2938-2940 (2017).

Figure 1

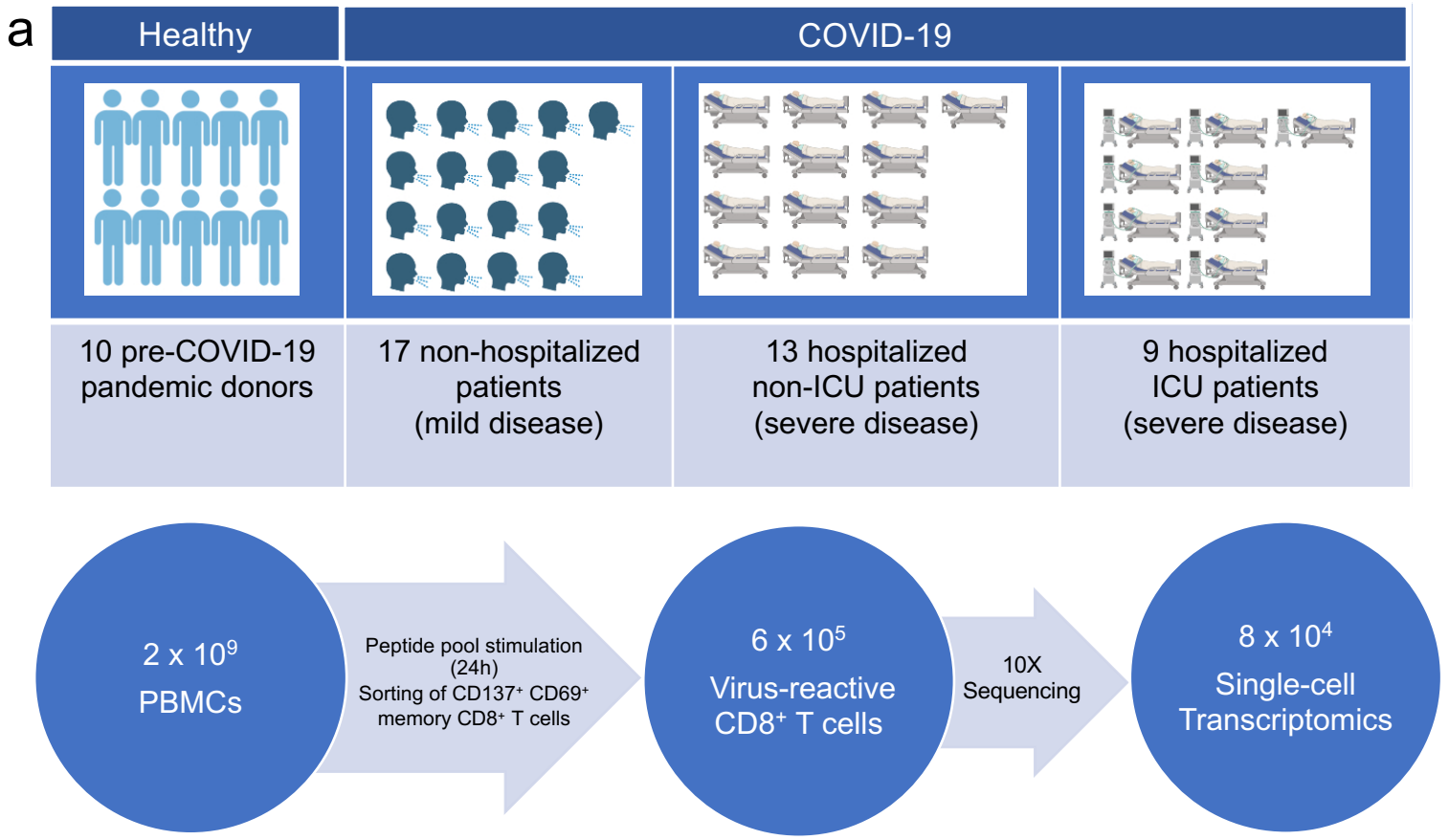

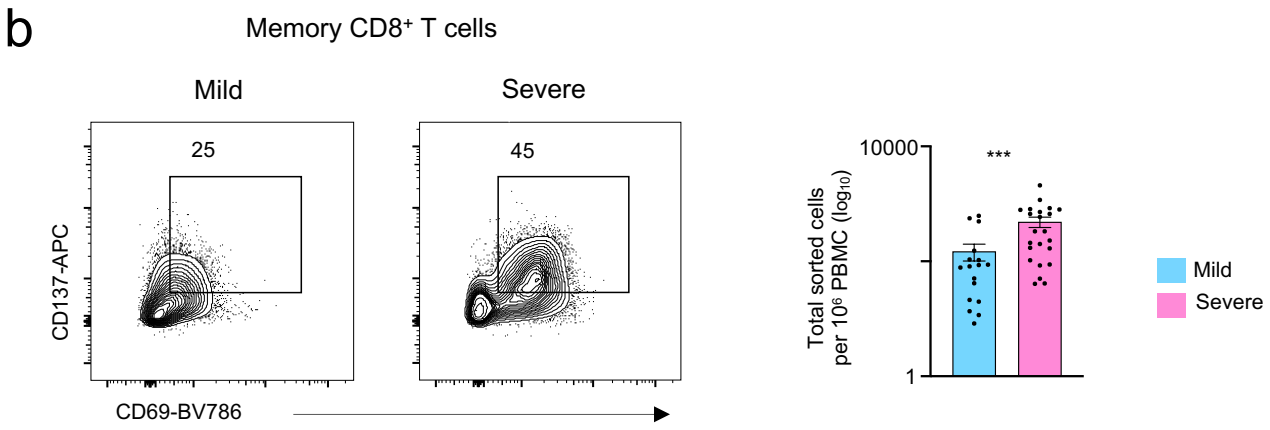

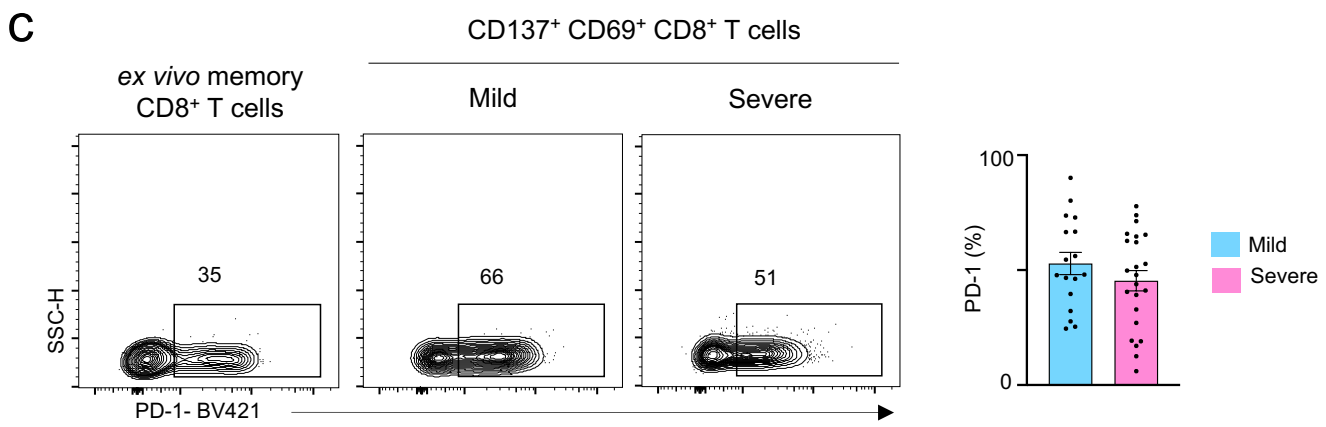

Figure 2

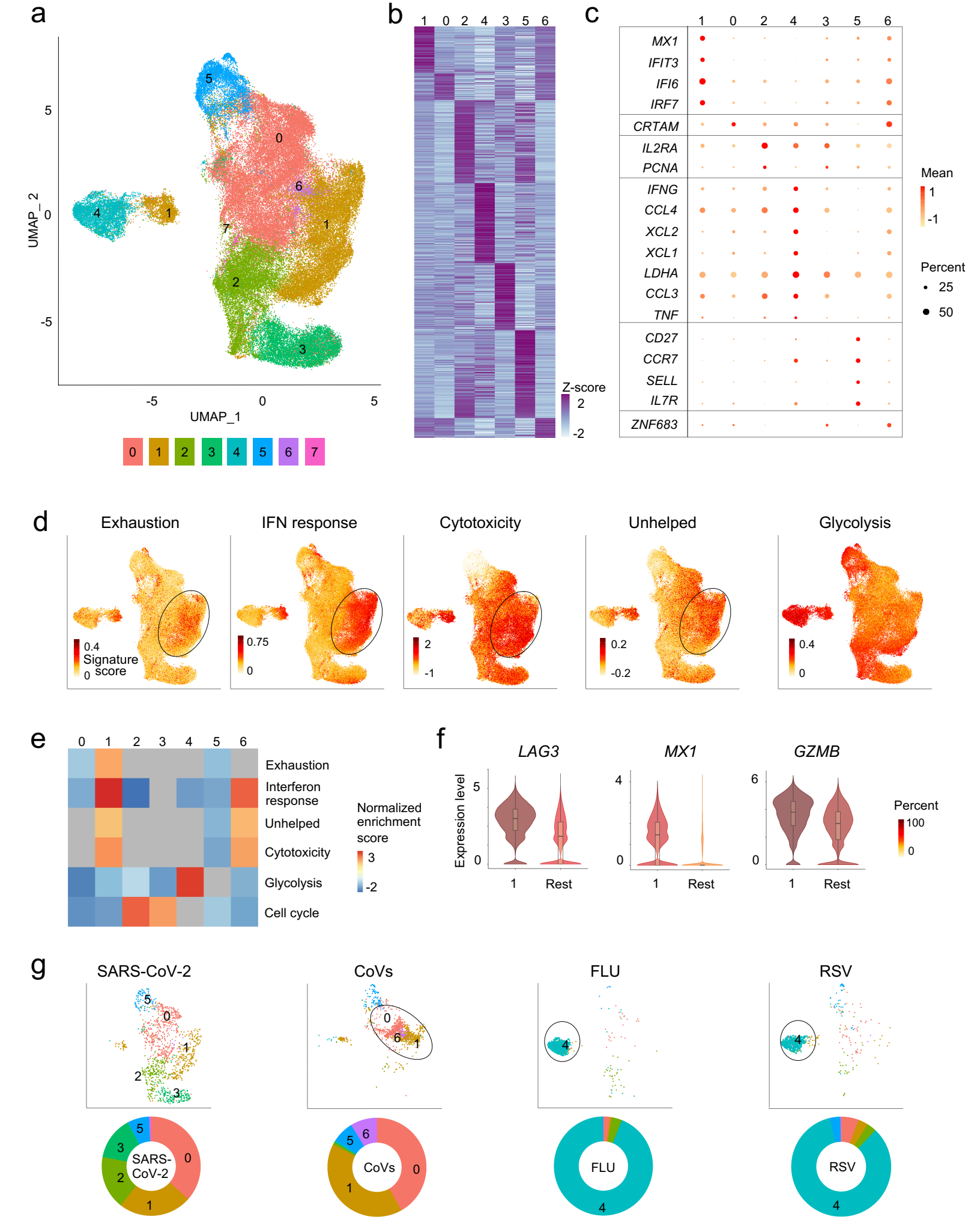

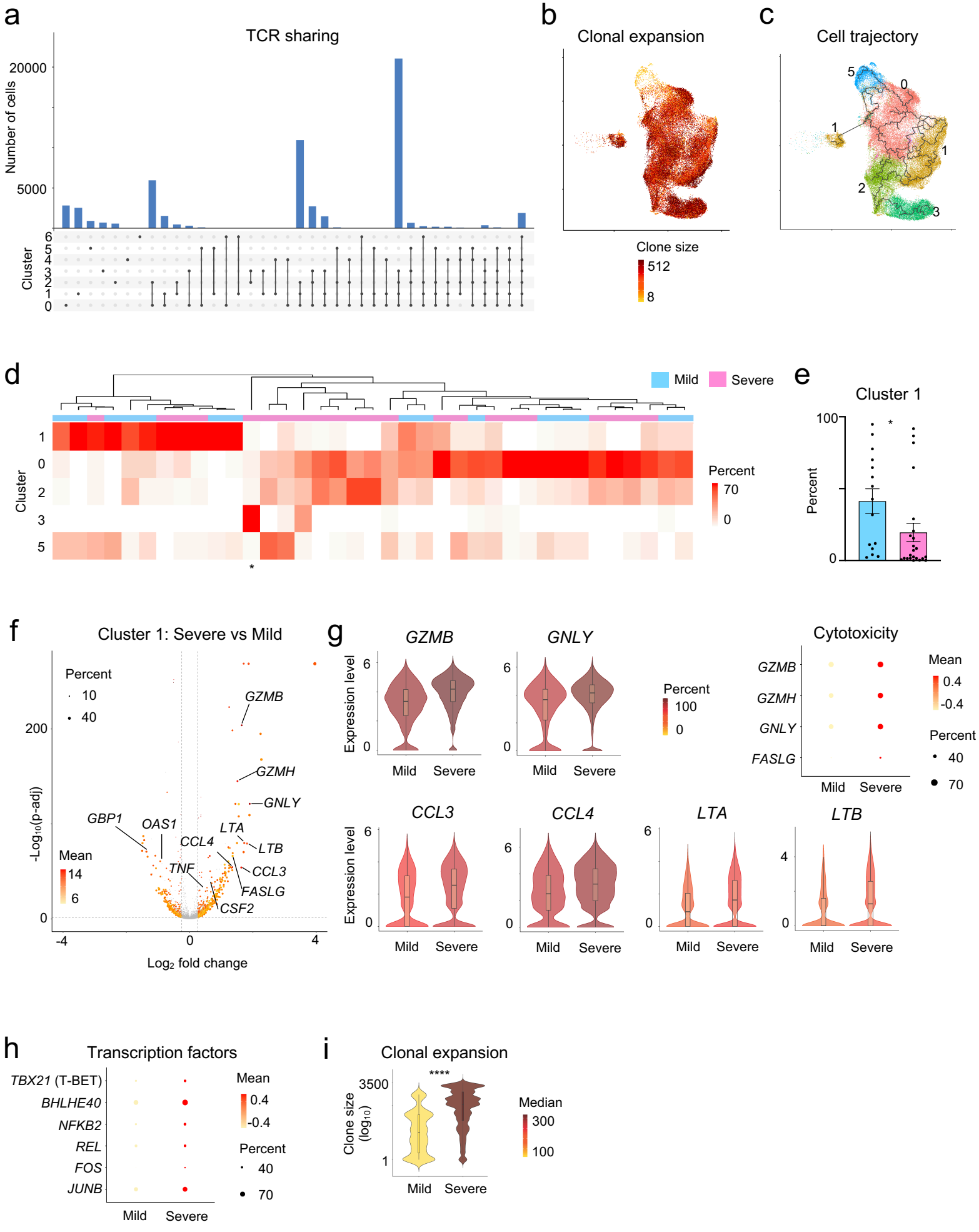

Figure 4

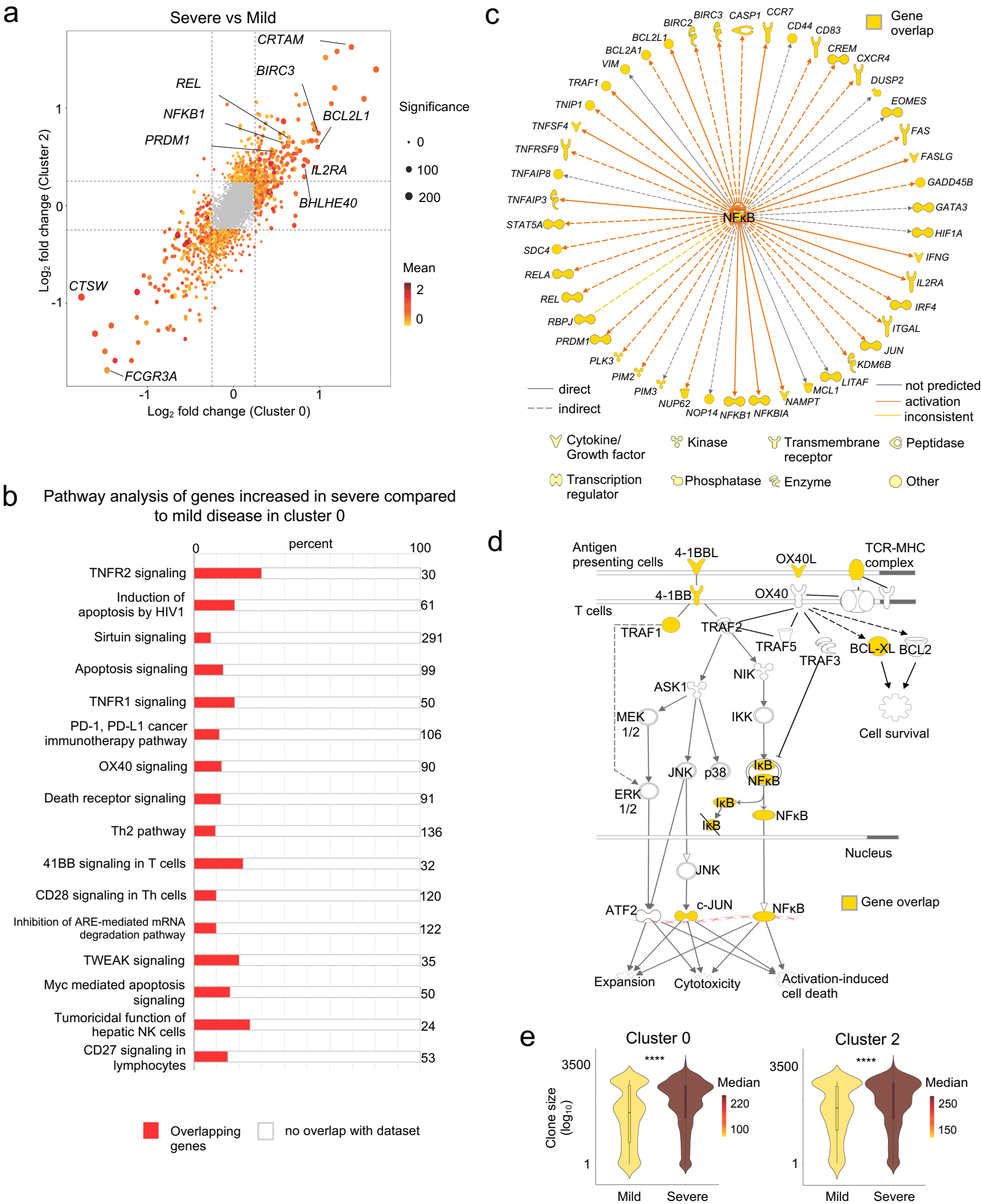
a
Severe vs Mild
CRTAM
BIRC3
REL
NFKB1
PRDM1
BCL2L1
IL2RA
BHLHE40
CTSW
FCGR3A
Log2 fold change (Cluster 2)
Log2 fold change (Cluster 0)
Significance
0
100
200
Mean
2
0
b
Pathway analysis of genes increased in severe compared to mild disease in cluster 0
percent
0
100
TNFR2 signaling 30
Induction of apoptosis by HIV1 61
Sirtuin signaling 291
Apoptosis signaling 99
TNFR1 signaling 50
PD-1, PD-L1 cancer immunotherapy pathway 106
OX40 signaling 90
Death receptor signaling 91
Th2 pathway 136
41BB signaling in T cells 32
CD28 signaling in Th cells 120
Inhibition of ARE-mediated mRNA degradation pathway 122
TWEAK signaling 35
Myc mediated apoptosis signaling 50
Tumoricidal function of hepatic NK cells 24
CD27 signaling in lymphocytes 53
Overlapping genes
no overlap with dataset
c
Gene overlap
NFκB
direct
indirect
not predicted
activation
inconsistent
Cytokine/ Growth factor
Kinase
Transmembrane receptor
Peptidase
Transcription regulator
Phosphatase
Enzyme
Other
d
Antigen presenting cells
4-1BBL
OX40L
TCR-MHC complex
4-1BB
OX40
T cells
TRAF1
TRAF2
TRAF5
TRAF3
BCL-XL
BCL2
NIK
ASK1
MEK 1/2
IKK
Cell survival
JNK
p38
IκB NFκB
ERK 1/2
IκB
NFκB
Nucleus
JNK
ATF2
c-JUN
NFκB
Gene overlap
Expansion
Cytotoxicity
Activation-induced cell death
e
Cluster 0
Cluster 2
****
Clone size (log10)
3500
1
Median
220
100
250
150
Mild
Severe

Extended Data Figure 1

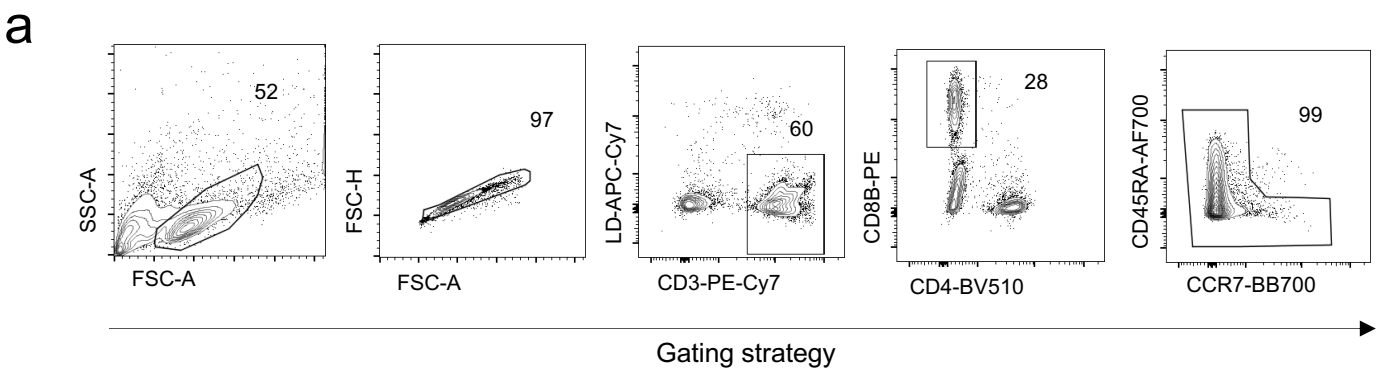

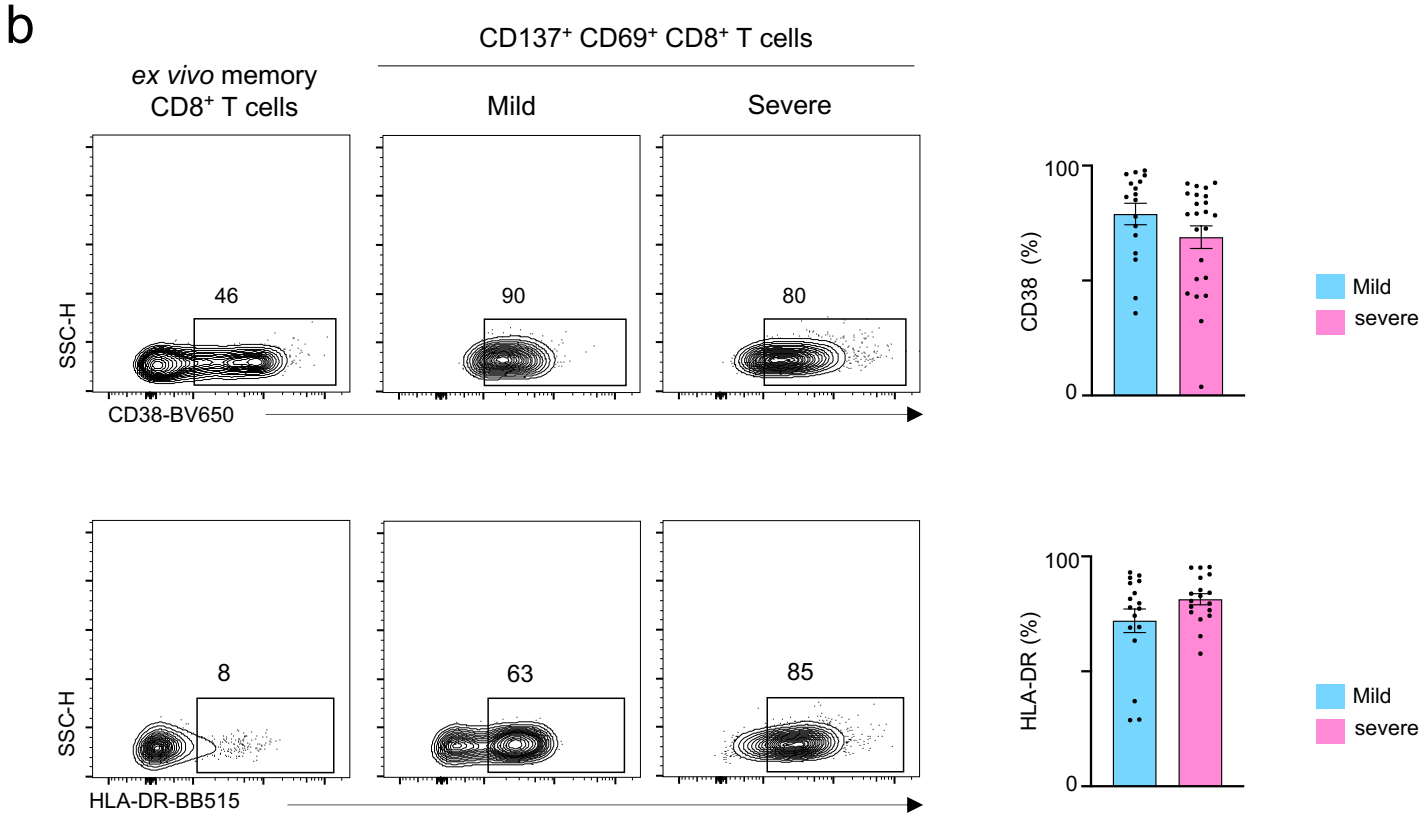

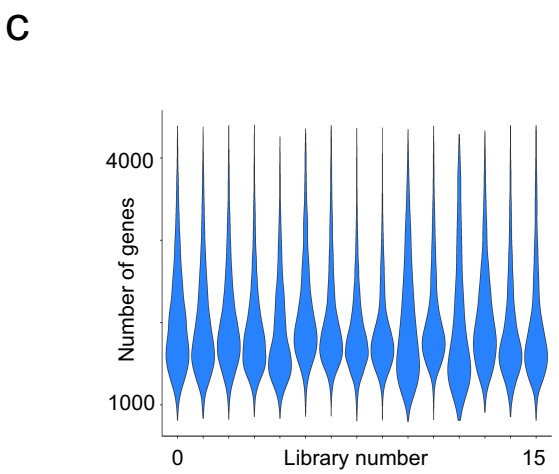

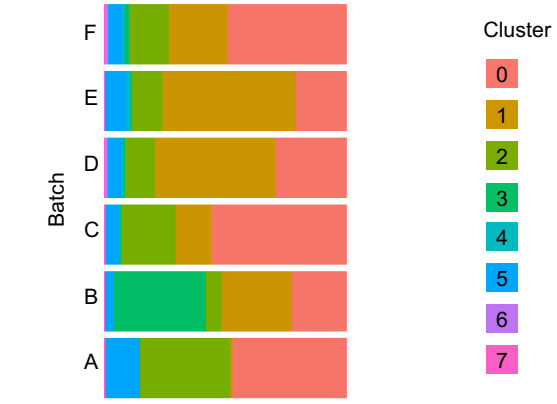

Extended Data Figure 2

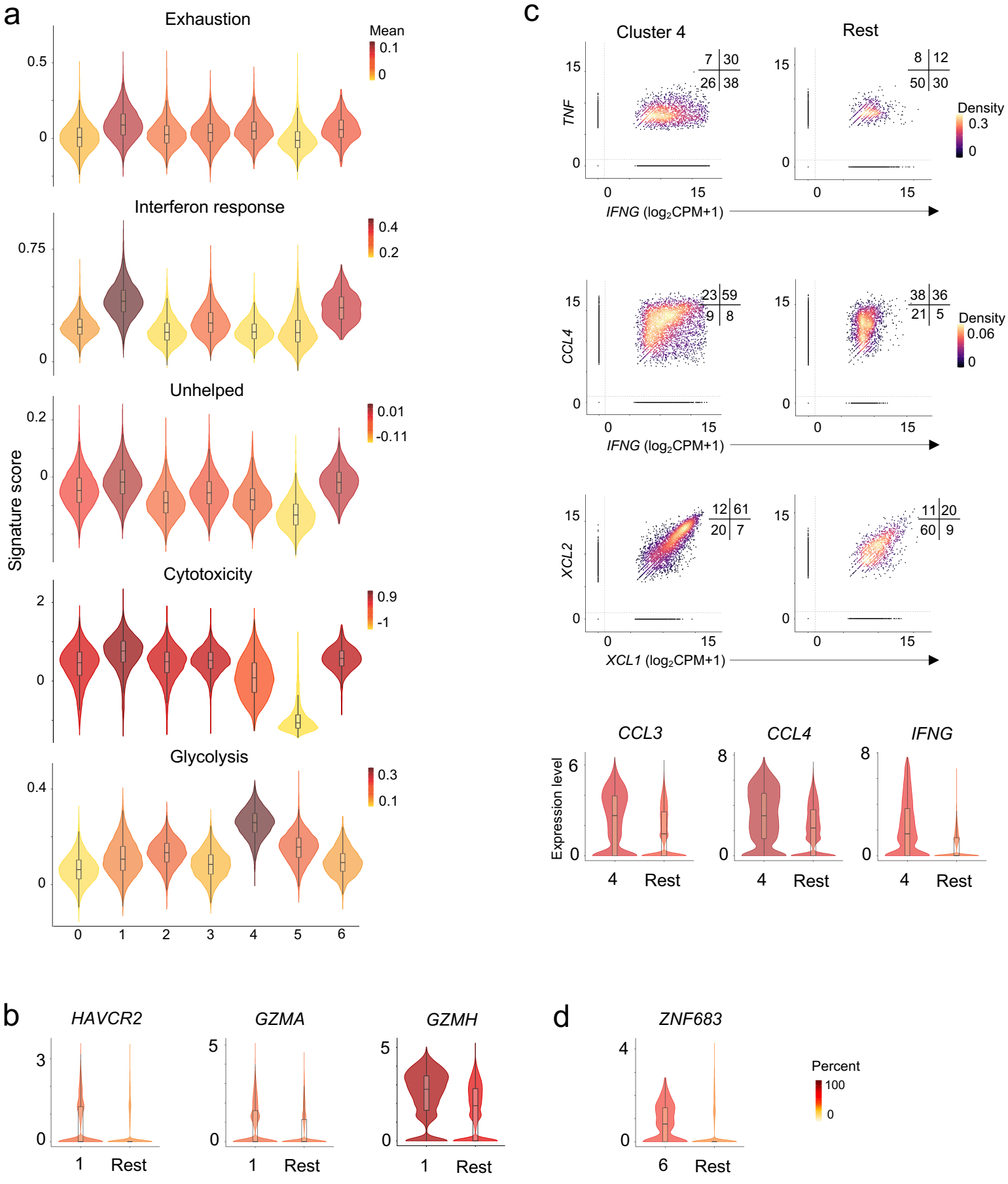

Extended Data Figure 3

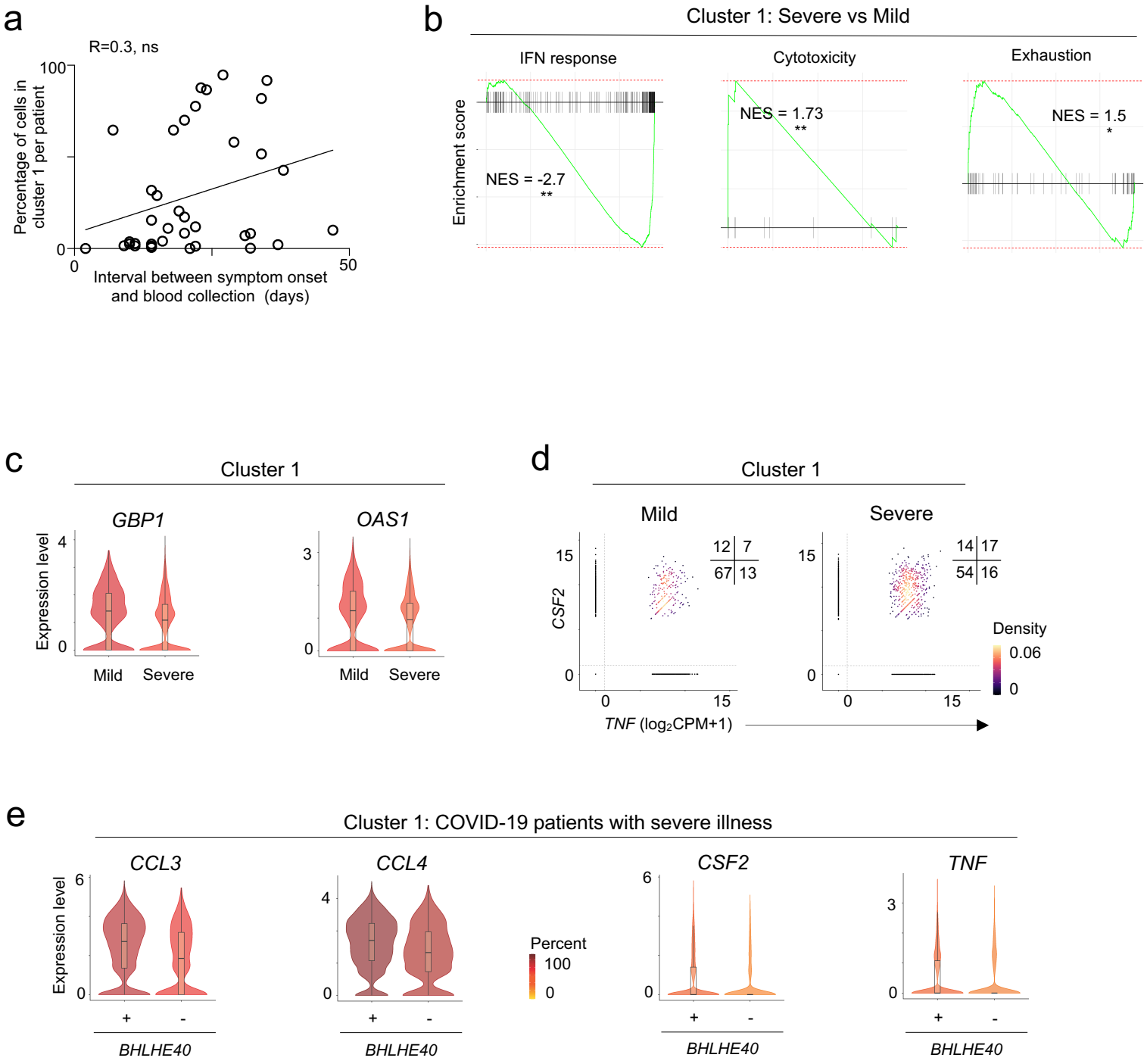

Extended Data Figure 4